BMES BIOMEDICAL ENGINEERING SOCIETY Check for updates

Original Article

Modeling of Tumor Growth with Input from Patient-Specific Metabolomic Data

HUNTER A. MILLER, 1 JOHN LOWENGRUB, 2,3 and HERMANN B. FRIEBOES 1,4,5,6

¹Department of Pharmacology and Toxicology, University of Louisville, Louisville, KY, USA; ²Department of Mathematics, University of California, Irvine, CA, USA; ³Department of Biomedical Engineering, University of California, Irvine, CA, USA; ⁴Department of Bioengineering, University of Louisville, Lutz Hall 419, Louisville, KY 40292, USA; ⁵UofL Health – Brown Cancer Center, University of Louisville, KY, USA; and ⁶Center for Predictive Medicine, University of Louisville, Louisville, KY, USA

(Received 31 July 2021; accepted 1 January 2022; published online 26 January 2022)

Associate Editor Aleksander S. Popel oversaw the review of this article.

Abstract—Advances in omic technologies have provided insight into cancer progression and treatment response. However, the nonlinear characteristics of cancer growth present a challenge to bridge from the molecular- to the tissue-scale, as tumor behavior cannot be encapsulated by the sum of the individual molecular details gleaned experimentally. Mathematical modeling and computational simulation have been traditionally employed to facilitate analysis of nonlinear systems. In this study, for the first time tumor metabolomic data are linked via mathematical modeling to the tumor tissue-scale behavior, showing the capability to mechanistically simulate cancer progression personalized to omic information obtainable from patient tumor core biopsy analysis. Generally, a higher degree of metabolic dysregulation has been correlated with more aggressive tumor behavior. Accordingly, key parameters influenced by metabolomic data in this model include tumor proliferation, vascularization, aggressiveness, lactic acid production, monocyte infiltration and macrophage polarization, and drug effect. The model enables evaluating interactions of interest between these parameters which drive tumor growth based on the metabolomic data. The results show that the model can group patients consistently with the clinically observed outcomes of response/non-response to chemotherapy. This modeling approach provides a first step towards evaluation of tumor growth based on tumor-specific metabolomic data.

Keywords—Metabolomics, Cancer, Personalized medicine, Mathematical modeling, Computational simulation.

Address correspondence to Hermann B. Frieboes, Department of Bioengineering, University of Louisville, Lutz Hall 419, Louisville, KY 40292, USA. Electronic mail: hbfrie01@louisville.edu

INTRODUCTION

The nonlinear response of an individual patient's tumor to a chosen therapy continues to confound the treatment of cancer. Although therapy efficacy may have been proven for patients with tumors of similar type and stage, and may also have been customized to specific tumor genetic characteristics, e.g., BRCA mutation, there is no guarantee that any particular untreated tumor will favorably respond to the same treatment. A major reason is that the tumor response is influenced by the individual tumor cell and microenvironment conditions, as well as patient physiological and life conditions. In order to provide for more accurate outcomes, the ability to gauge and incorporate these conditions into treatment expectations is crucial. Due to the dysregulation of metabolism in cancer, metabolomics in particular has shown promise to provide critical information regarding cancer evaluation and prognosis. ⁷ Ideally, metabolomics coupled with other molecular information, such as genomics, transcriptomics, and proteomics would describe individual patient tumor conditions as a set of "signals" that reflect individual tumor conditions. However, the amount of data generated by such analyses is large, and can be difficult to interpret.⁴³

To tackle this challenge, mathematical modeling and computational techniques have been employed to study the nonlinear behavior of tumors. Advances in metabolomics and mathematical modeling, as well as in the estimation of model parameter values based on metabolome data were reviewed in Ref. 67, focusing on

metabolic reaction networks and kinetic models. The role of mathematical modeling in attaining an enhanced understanding of cancer metabolic reprogramming as well as to identify potential therapeutic interventions was recently reviewed. ⁴⁹ In particular, Wnt signaling has been linked via mathematical modeling to metabolism patterns in colon cancer. ³³ Although metabolism at the cellular scale has been modeled, (e.g., Refs. 50, 62, 63), along with the associated networks, ⁸² it has been challenging to link the metabolic to the tissue scale.

Part of the challenge lies in linking metabolomic measurements to mathematical model parameters. A model system designed to simulate tumor behavior would ideally provide sufficient dynamic range to represent various biological conditions while also translating biological measurements into (usually dimensionless) model parameters. In this study, a model system is constructed to mechanistically bridge from patient tumor metabolomic measurements to mathematical model parameters. As proof of concept, the model parameters are calibrated to simulate the progression of lung tumors. Biologically relevant models must include an adequate number of parameters to provide useful predictions. We propose a set of parameters which represent an adequate number to simulate tumor growth based on metabolomic data. The ultimate goal is for such a system to serve as a prognostic tool by projecting tumor behavior into future time, so that the response to particular treatment modalities could be evaluated and selected for efficacy prior to patient administration.

MATERIALS AND METHODS

Vascularized Tumor Growth

We use a tumor growth component based on a 2D continuum representation of tissue, as described in Refs. 41, 79 while the angiogenesis component represents blood vessels as discrete elements, as described in Ref. 48. Briefly, as the tumor grows within a vascularized environment, the tissue has heterogeneous access to oxygen and nutrients diffusing from the vasculature. Oxygen and nutrients are transported to the tumor from the location of extravasation from the vasculature. The interstitial flow of oxygen and nutrients is influenced by tissue pressure and by distance from the nearest vessels. Neo-vessel sprouts arise from the host vasculature, whose epithelial cell tips migrate semi-stochastically towards a gradient of tumor angiogenic factor (TAF) produced by tumor tissue. The main equations of the vascularized tumor growth model in Refs. 41, 79 are summarized in Supplement.

Tumor Aggressiveness

Tumor aggressiveness G is a non-dimensional parameter that represents the ratio of cell proliferation to the rate of tissue relaxation due to cell-cell adhesion. Assuming uniform cell-cell adhesion throughout the tumor, G is incorporated as a surface-tension like jump boundary condition at the tumor-host interface⁴¹:

$$[P] = (P_{\text{inner}} - P_{\text{outer}}) = \frac{1}{G}\kappa, \tag{1}$$

where κ is the mean curvature of the interface, and P is the oncotic pressure representing the balance of the intra-tumoral (P_{inner}) and extra-tumoral (P_{outer}) pressures. Thus, higher proliferation or lower cell-cell adhesion would raise the tumor aggressiveness, meaning that the tumor would overall push stronger (be more invasive) into its surroundings.

Tumor-Associated Macrophages

Tumor-associated macrophages (TAMs) of two different subtypes are simulated in the vascularized tumor microenvironment, as described in Refs. 38, 42. Briefly, monocytes extravasate from the vasculature following local concentration of chemoattractants secreted from hypoxic tissue, stimulating them to migrate towards regions of tissue hypoxia. Monocytes undergo polarization into M1 (tumoricidal) or M2 (tumorigenic) subtypes in the vicinity of the tumor microenvironment based on the concentration of chemokines released by proliferating and hypoxic tumor cells, and affect the net tumor proliferation. 10,36,37 As in Ref. 42, pressure, oxygen, and chemoattractant gradients affect the semi-stochastic movement of monocyte precursors and the M1 and M2 macrophage subtype movement through the interstitium.

Lactic Acid

Enhanced lactic acid production by anaerobic glycolysis (Warburg Effect) in cancer is well known and contributes to a low pH within the tumor microenvironment. Additionally, lactic acid is known to be uptaken by cancer cells through monocarboxylate transporters (MCTs) and utilized as an energy substrate. ⁶⁴ In the model, lactic acid is produced by proliferating and hypoxic tumor cells and diffuses in the surrounding tissue. It can be uptaken by tumor cells and wash out of the tissue into the vasculature, which altogether represent the decay. Lactic acid produced for every mole of glucose during anaerobic respiration ⁷⁷:



$$\begin{split} 0 &= \nabla \cdot (D_{\text{Lac}} \nabla L) + \overline{\lambda}_{\text{production}}^{\text{Lac}} (1 - L) - \overline{\lambda}_{\text{washout}}^{\text{Lac}} \mathbf{1}_{\text{vessel}} \\ &- \overline{\lambda}_{\text{uptake}}^{\text{Lac}} L, \end{split} \tag{2}$$

where D_{Lac} is the diffusivity, L is the local concentration of lactic acid, $\overline{\lambda}_{\text{production}}^{\text{Lac}}$ is the production rate, $\overline{\lambda}_{\text{washout}}^{\text{Lac}}$ is the rate of washout, and $\overline{\lambda}_{\text{uptake}}^{\text{Lac}}$ is the cellular uptake rate (assumed to be on the same order of magnitude as that of oxygen). The production rate of lactic acid is concentration dependent, as it has been shown that cancer cells have the ability to adjust their metabolic behavior by altering lactic acid production to maintain a range of pH within the microenvironment. 46

For simplicity, it is assumed that lactic acid production $\overline{\lambda}_{production}^{Lac}$ gradually decreases as the level of oxygen and nutrients σ increases towards areas of higher vascularization:

$$\overline{\lambda}_{\text{production}}^{\text{Lac}} = \begin{cases}
1 - \sigma & \text{in proliferating tissue} \\
2\sigma & \text{in hypoxic tissue} \\
0 & \text{in necrotic tissue}
\end{cases}$$
(3)

Since the molar mass of lactic acid (\sim 90 g/mol) is on the order of magnitude of oxygen (16 g/mol), the diffusion constant $D_{\rm Lac}$ is for simplicity assumed to be on the same order of magnitude as oxygen. Accordingly, lactic acid diffuses through the host and tumor tissue relatively uninhibited by the ECM. Similarly, the lower bound rate of lactic acid uptake by cells is assumed to be on the same order of magnitude as oxygen.

Chemotherapy

A number of chemotherapeutic agents are routinely administered to non-small cell lung cancer (NSCLC) patients. To test the proposed model linking metabolomic data to tissue-scale behavior, we chose to simulate response to cisplatin (CDDP), a representative NSCLC drug. The transport of drug c with diffusivity D_c was simulated from the position of extravasation from the vasculature. Uptake by tumor and normal cells and wash-out from the interstitial space were included as a combined effect in the rate $\lambda_{c,\text{uptake}}$, which reflects the drug half-life (assumed to be similar to the half-life in plasma) 73 :

$$0 = \nabla \cdot (D_c \nabla c) + \lambda_{c,ev}(\mathbf{x}, \mathbf{t}, \mathbf{1}_{vessel}, \mathbf{p_i}, \mathbf{c}) - \lambda_{c,uptake} \mathbf{c}$$
(4)

A constant drug extravasation transfer rate $\lambda_{c,TR}$ from the vasculature was assumed ⁷⁰:

$$\lambda_{c,ev} = \lambda_{c,TR} \mathbf{1}_{vessel}(\mathbf{x}, \mathbf{t}) \left(\mathbf{1} - \mathbf{k}_{p,i} \frac{\mathbf{p}_{i}}{\mathbf{p}_{e}} \right) \left(\frac{\mathbf{C}_{c,t}}{\overline{\mathbf{C}}_{c}} - \mathbf{c} \right) \quad (5)$$



where $\lambda_{\rm c,TR}$ is the constant transfer rate from pre-existing and new vessels, $1_{\rm vessel}({\bf x},{\bf t})$ equals 1 at vessel locations and 0 elsewhere, $k_{\rm p,i}$ represents the weight of convective transport component of small molecules, $p_{\rm i}$ is interstitial fluid pressure (IFP), and $p_{\rm e}$ is effective pressure (IFP at which there is no net volume flux out of the vasculature). Drug concentration in the vasculature is initially $\overline{C}_{\rm c}$, where extravasation follows first order kinetics for a constant drug infusion: $C_{\rm c,t} = 1 - e^{-\alpha t}$, with α based on an average CDDP half-life of 0.5 h. 35

Metabolomic Data

The metabolomic datasets based on lung tumor core biopsies from 23 patients in Ref. 53 (available in Metabolomics Workbench Repository, record ST001527) were used to illustrate the study methodology for patient-specific tumors. These data are described in further detail in Ref. 53. Briefly, patient tumor tissue samples were processed by liquid-liquid metabolite extraction and analyzed by 2DLC-MS with negative and positive ion modes. 2DLC-MS data was presented as an alignment table for each batch with retention time, m/z, signal intensity, stable isotope labeling, name of identified metabolite, and database used for metabolite identification. After combining data from positive and negative ion modes, a preliminary step to handle missing values was performed by removing features which contained more than 50% missing values. This resulted in a data set of 66 metabolites with approximately 21.8% missing values. The data were normalized by a log transformation and imputed by probabilistic principal component analysis (PPCA).

RESULTS

Linking of Metabolomic Data to Model Parameters

A baseline (representative) tumor nodule was first created *in silico* by calibrating the model parameters to lung tumor experimental data, and a range for the parameter values around baseline was determined (Supplement). The main model parameters affected by metabolomic data include the rate of proliferation, angiogenesis, lactic acid production, drug effect, monocyte production and polarization to the Type 1 and Type 2 macrophage phenotype. In turn, the lactic acid concentration locally modulates the polarization of monocytes to the Type 2 macrophage, while the overall lactic acid within the tumor tissue influences the tumor aggressiveness. Lactic acid is also an important contributor to angiogenesis. ¹⁹ Table 1 summarizes a set of relevant metabolites detected in lung tumor tis-

TABLE 1. Potential effect of NSCLC metabolites on model parameters.

	Model parameters								
Metabolite	Tumor prolif- eration	Type 1 mac- rophage	Type 2 mac- rophage	Angio-ge- nesis	Drug effect	Lactic acid pro- duction	Monocyte pro- duction	Refs.	
Acetyl-L-carnitine ^A N8-acetyl-sper- midine ^A	A			A				14, 83 56	
Arginine ^A	▲ a,b	A	▼					58, 68,	
Creatinine ^A Cystine ^B Fumarate ^B Glutamic acid ^B Glutamine ^B Glutaric acid ^A	▼ °	Y	*	₫	A			85 32, 60 13, 31 81, 84 20 66, 75 34	
Hydroxybutyric acid ^A Hydroxyphenyl-lac-	A						▼ e	27 9	
tic acid ^A Inosine ^A Isoleucine ^B Lactic acid ^A Lysine ^B Malonic acid ^A Methionine ^B Methionine sulfox-	▲ ▼			A	▲ a	▲ ▼ ^h		11 2, 4 19 80 6, 30 72 39	
ide ^B N3,N4-dimethyl-∟- arginine ^B		A	▼					76	
Ornithine ^A Phenylalanine ^B Proline ^A Pyruvate ^A	A	A	▼	A			▼ ⁱ	58 61, 66 22, 47 1, 28,	
Salicylic acid ^A Serine ^B	•	▲ ^j	▼ j				▼	65 26 40, 45,	
Succinate ^A Threonine ^B Tryptophan ^B Urea ^B	∆b	Y A A	A Y Y				≜ ^k	57 78 25 68 54	
Uric acid ^A Valine ^B	▲ ⁵ ▼f	•	▼					23 3	

Metabolites detected in lung cancer patient tumor samples⁵³ (leftmost column), and their potential promotion (▲) or abatement (▼) of key model parameters (top row). Biological significance of the metabolites to NSCLC is indicated from literature sources (rightmost column). ^APromoting tumor progression; ^Bpromoting tumor control.



^aArginine is a "conditionally essential" amino acid involved in the synthesis of polyamines, which promote tumor growth, invasion and metastasis⁵⁸ and is also involved in immune system activation.^{68,85}.

^bAlthough these metabolites promote immune system activation, they are considered to favor tumor progression because the involvement in tumor growth, migration, and contribution to cancer risk/mortality is considered a stronger overall effect.

^cIncreased levels of cystine may be the result of decreased intracellular conversion to cysteine for catabolic usage¹³ and glutathione synthesis,³¹ which would reflect decreased cancer growth.

^dAccumulation also leads to persistence of hypoxia-inducible factors in the microenvironment, ⁸¹ potentially promoting angiogenesis. In the context of chemotherapy, angiogenesis combined with potentiation of the drug effect by fumarate is assumed to improve the overall tumor drug response. ^eGeneral effects of immune system activation or suppression are simulated by changing the monocyte production rate. ⁹.

^fAccumulation is assumed to reflect decreased cancer growth.

⁹Promotes epithelial-mesenchymal transition (EMT), which involves enhanced migration, invasiveness, elevated resistance to apoptosis, and increased ECM production, ²⁹ overall decreasing the drug effect.

^hRelieves stress caused by acidic microenvironment³⁹; simulated in the model by lowering the lactic acid production rate.

ⁱIncreased levels of ornithine may be the result of increased arginine, which promotes tumor growth and immune system activation. ^{58,68,85}.

Promotes adaptive immune activity, 40 simulated in the model by enhanced anti-tumor macrophage polarization..

kIncreases monocyte proliferation, simulated with higher overall macrophage numbers. 54.

sue samples,⁵³ and highlights the corresponding model parameters potentially affected by these metabolites, as has been established from previous biological observations. Individual metabolites can overall promote tumor progression or tumor control via the combination of increasing (promoting) or decreasing (abating) particular parameters. Thus, each metabolite can have "pro-parameter" and "anti-parameter" effects.

A flowchart summarizing the process for determining parameter values based on particular metabolomic data is shown in Fig. 1.

Determination of Model Parameter Values from Particular Metabolomic Data

Starting with a 2DLC-MS data set, as in Ref. 53, the weighted coefficients can be determined via a Spearman correlation analysis of experimentally measured metabolite intensities to the clinical response assessment, such as the Response Evaluation Criteria in Solid Tumors Group (RECIST), 21,74 or by the Variable Importance in Projection (VIP) scores obtained from a PLS-DA model and scaling of these scores to represent the fraction of their contribution to the parameter of interest. It is assumed for each metabolite

in a set of patient metabolomic data that the weighted coefficient W and intensity value M^{71} as described in Fig. 1 are positive; if not, they are first rescaled as follows:

$$W = abs(w) \tag{6}$$

$$M = m + abs(m_{\min}) \tag{7}$$

where for each metabolite, w is the weighted coefficient, m is the transformed intensity value, and m_{\min} is the minimum intensity value in the dataset. Transformations are generally applied to a dataset to normalize and enable proper statistical analysis. For each parameter, the metabolite weighted coefficients (W) are rescaled to a scale of 0 to 1 by dividing each value by the sum of all coefficient values relevant to the given parameter:

$$\overline{W} = \frac{W}{\sum_{i=1}^{n} W_i} \tag{8}$$

where for each metabolite, \overline{W} is the rescaled weighted coefficient and n is the total number of metabolites associated with the parameter (as listed in Table 1). To determine the values for a particular model parameter

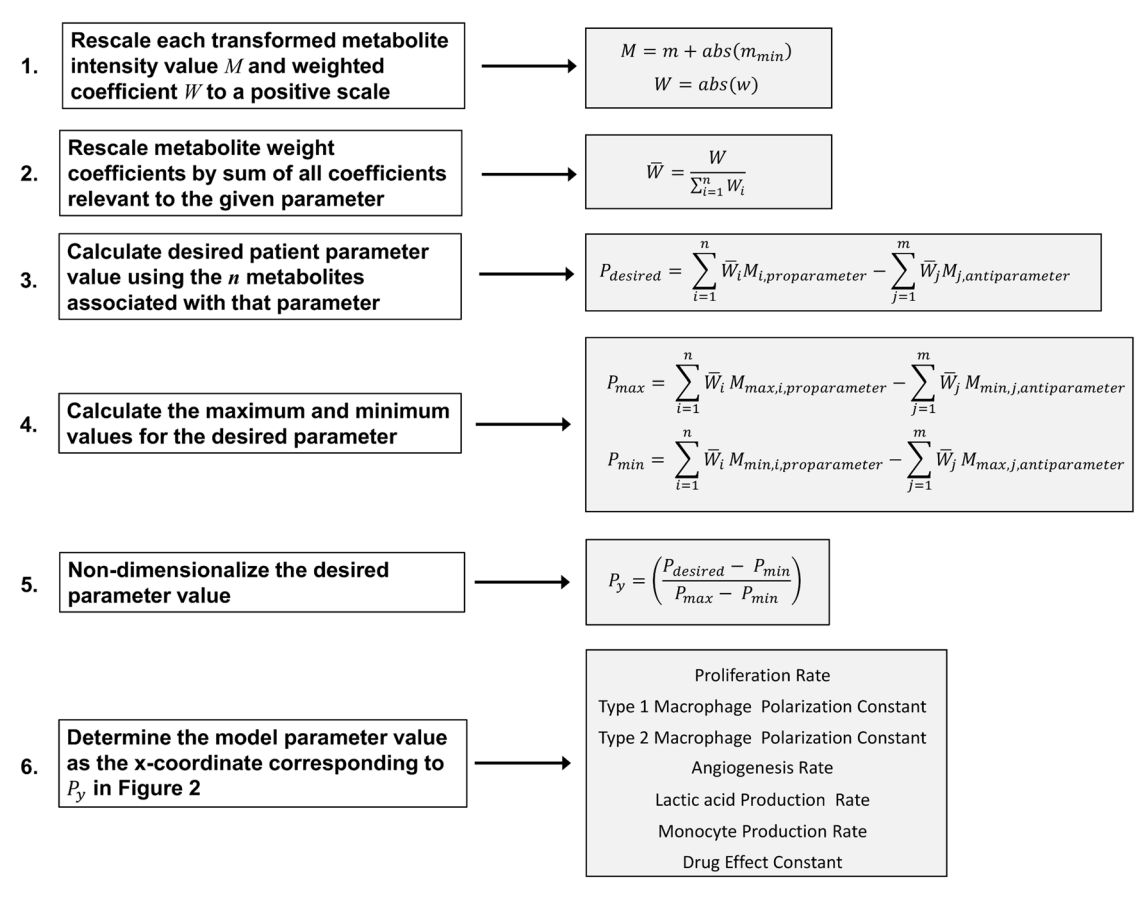


FIGURE 1. Workflow for coupling metabolomic data to model parameter values.



 P_{desired} (Table 1, top row) based on the associated metabolomic data, these data are first non-dimensionalized to values P_{v} :

$$P_{y} = \left(\frac{P_{\text{desired}} - P_{\text{min}}}{P_{\text{max}} - P_{\text{min}}}\right) \tag{9}$$

where P_{\min} and P_{\max} are the minimum and maximum values calculated across all samples for the desired parameter. P_{desired} , P_{\max} , and P_{\min} are calculated as the weighted sums of pro-parameter metabolites minus the weighted sums of the anti-parameter metabolites of the corresponding metabolite measurements M, M_{\max} and M_{\min} associated with the desired parameter (Table 1):

$$P_{\text{desired}} = \sum_{i=1}^{n} \overline{W}_{i} M_{i,\text{proparameter}} - \sum_{j=1}^{m} \overline{W}_{j} M_{j,\text{antiparameter}}$$
(10)

$$P_{\text{max}} = \sum_{i=1}^{n} \overline{W}_{i} M_{\text{max},i,\text{proparameter}} - \sum_{i=1}^{m} \overline{W}_{i} M_{\text{min},j,\text{antiparameter}}$$
(11)

$$P_{\min} = \sum_{i=1}^{n} \overline{W}_{i} M_{\min,i,\text{proparameter}}$$
$$-\sum_{i=1}^{m} \overline{W}_{i} M_{\max,i,\text{antiparameter}}$$
(12)

where M_{max} and M_{min} are the rescaled maximum and minimum values for a particular metabolite associated with the desired model parameter, and n and m are the total number of pro-parameter and anti-parameter metabolites respectively associated with this parameter (as listed in Table 1).

The weighted coefficients (i.e., relative contribution of specific metabolites towards the dependent variable) can be objectively determined by applying multivariable (e.g., partial least squares discriminant analysis (PLS-DA)) or univariable (e.g., correlation analyses) statistical techniques to the metabolomic dataset, as has been previously shown. 12,59

A representative set of non-dimensionalized P_y values is shown in Fig. 2. The lines are generated by plotting the model-generated values at 400 h of tumor growth for every metabolism-associated model parameter (see Supporting Information). The parameters were changed one at a time while holding other parameters constant at their baseline values. The time of 400 h was selected because by that time the simulated tumor growth had attained a steady rate of increase (Supplementary Fig. 1). Given P_y on the y-axis, one can then interpolate the value for a particular

model parameter by mapping (or fitting) to the *x*-axis. Linear or logarithmic functions were found to adequately map the experimentally measured metabolite values to the model parameter space.

Variation in Metabolic Dysregulation

Model parameter values representing a range of minimum to maximum metabolic dysregulation (from LOW to HIGH, with BASELINE in between) were chosen in order to simulate the corresponding extremes of metabolic-influenced tumor growth. The range of parameter values listed in Table 2 defines a set of bounds for the values that could be utilized for NSCLC patient-specific tumor simulations based on the dataset in Ref. 53. The ranges were determined by interpolating values that covered the capability of the model to simulate a range of biologically relevant vascularized tumor growth. In this study, as well as in previous work using these types of models, 8,15,24,42,79 we have found that values in these ranges are adequate to evaluate the parameters driving this growth. Type 1 macrophages have the same LOW and MEDIUM values, and Type 2 macrophages have the same MEDIUM and HIGH values due to the calibration of macrophage polarization to maintain tumor growth consistent with the baseline case, as described earlier. The macrophage types are coupled, and their ratio determines the overall range of interactions with the tumor tissue. For angiogenesis, the BASELINE case already represents a highly vascularized condition.⁷⁹

Tumor radius and vessel surface area are shown over time for the three cases in Figs. 3a and 3b. At 400 h, the HIGH case had 850% of the vasculature and 220% of the radius of the LOW case. In Figs. 3c–3e, the proliferating, hypoxic, and necrotic tissue fractions are shown to highlight the differences in tumor tissue heterogeneity over time. At 400 h, the HIGH case had 51, 375, and 124% of the proliferating, hypoxic and necrotic tissue regions of the LOW case, respectively. The ratio of Type 1 to Type 2 macrophages is shown in Fig. 3f (the HIGH case has no Type 1 macrophages, Table 2).

Simulation of Particular Tumors In Silico

To illustrate the methodology for patient-specific tumors, we simulated the growth phase of a tumor incorporating metabolomic data (Table 3) previously measured from a lung cancer tumor core biopsy. These data represent log transformed metabolite intensity values, e.g., measured from liquid chromatography mass spectroscopy (LC-MS). Log transformation is commonly applied to biological data to center it and correct for heteroscedasticity. The



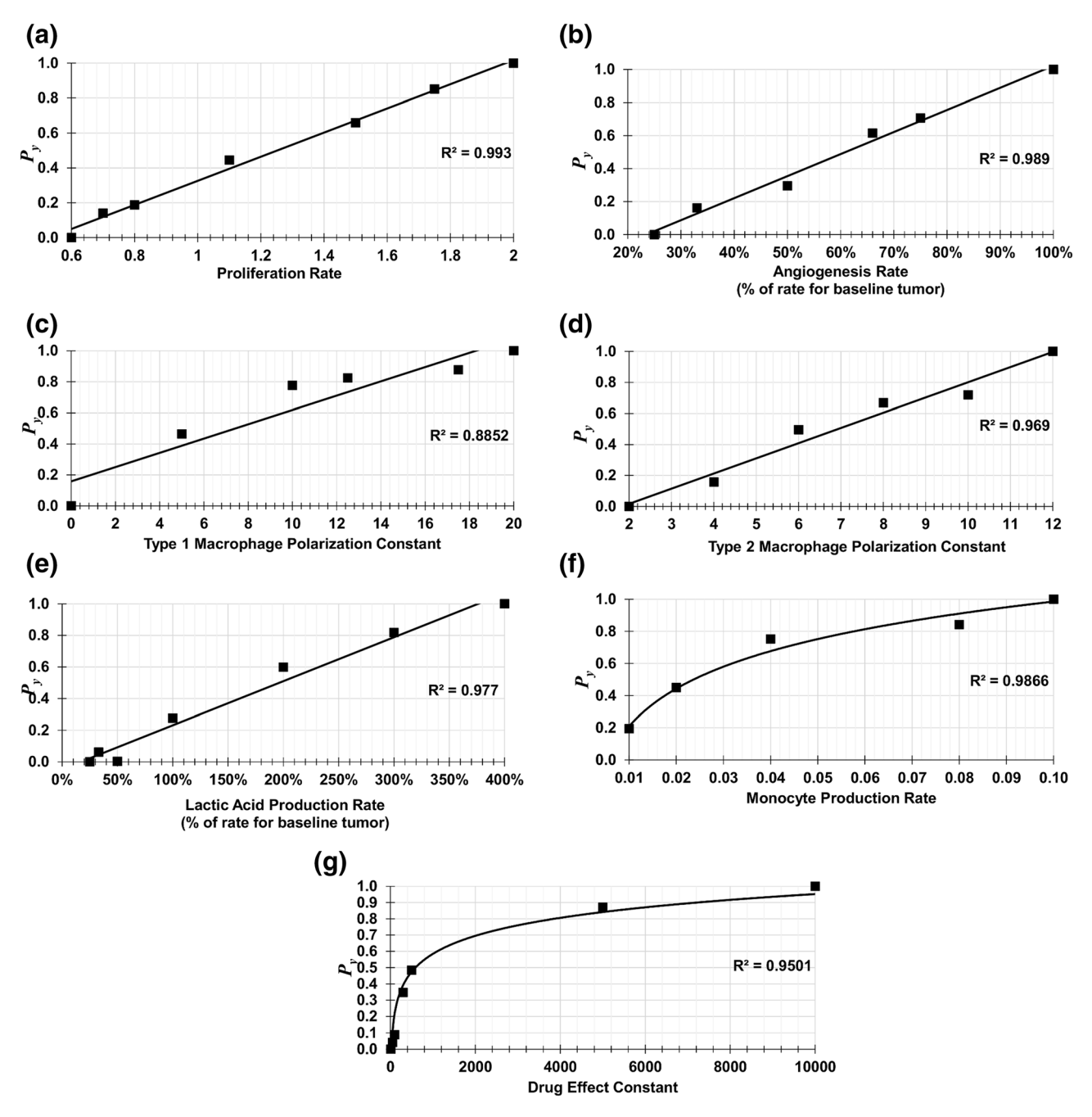


FIGURE 2. Parameter curves showing P_y vs. parameter values. These graphs map a set of patient metabolomic data (y-axis, rescaled to values between 0 and 1) to the parameter space of the model (x-axis).

parameter values are calculated in the following manner, based on the workflow outlined in Fig. 1: First, the transformed intensity value for each metabolite (M) is rescaled to a positive scale by summing the absolute value of the largest negative value (m_{min}) to all intensities (across all metabolites) so that the largest negative value corresponds to zero (Fig. 1, Step 1). A variety of methods could be used to determine the weighted coefficients, including PLS-DA VIP scores, Spearman correlation coefficients, and PLS-DA load-

ings. Spearman correlation coefficients are found by analyzing clinical response as a function of the transformed metabolite intensities. Similarly, in PLS-DA the transformed metabolite intensities are used as the predictor variables and clinical outcome can be used as the response variable. All metabolite weighted coefficients are rescaled to a positive scale by taking the absolute value of each weighted coefficient (Fig. 1, Step 1). Then, the metabolite weight coefficients (W) are rescaled to range from 0 to 1 by dividing each value by



TABLE 2. Ranges for model parameter values.

Model parameter	LOW	BASELINE	HIGH	SAMPLE
Proliferation rate	0.600	1.100	2.000	1.356
Type 1 macrophage polarization constant	20.000	20.000	0.000	9.863
Type 2 macrophage polarization constant	2.000	12.000	12.000	8.075
Angiogenesis rate ^a	25.0	100.0	100.0	66.7
Lactic acid production rate ^a	25.0	100.0	400.0	192.4
Monocyte production rate	0.005	0.020	0.100	0.020
Drug effect constant	1.0E+04	100.0	10.0	805,3

Model parameter values chosen to define a range of metabolic-influenced tumor growth and drug response, in order to simulate LOW, BASELINE, and HIGH metabolic dysregulation. For comparison, SAMPLE values are calculated for a representative patient in the dataset. aShown as % of the corresponding rate for the baseline tumor.

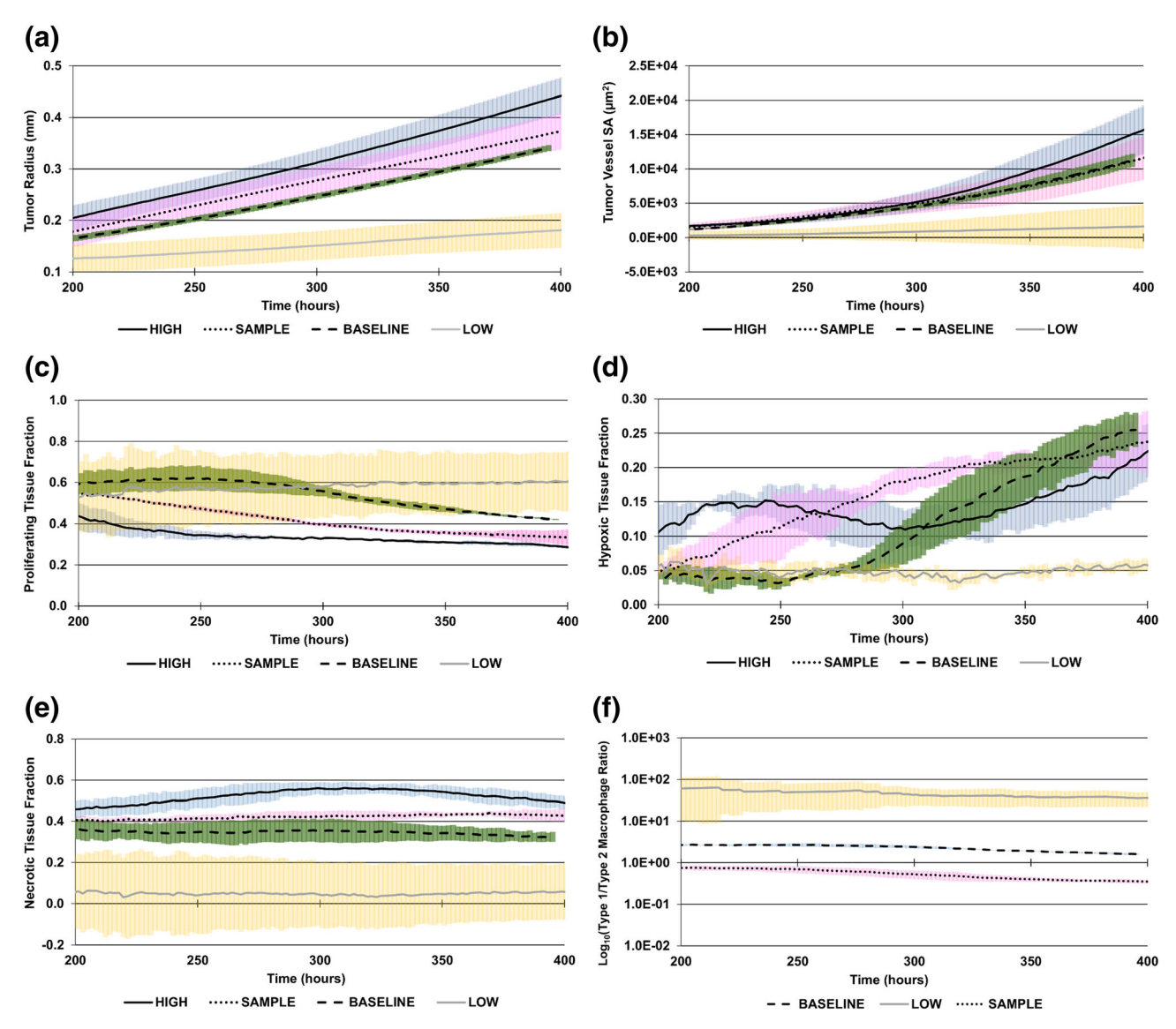


FIGURE 3. Curves establishing a range of metabolic dysregulation during tumor growth. LOW: minimum theoretical dysregulation (yellow error bars); BASELINE: dysregulation based on baseline tumor values (green error bars); HIGH: maximum theoretical dysregulation (blue error bars); SAMPLE: a representative patient case for illustration purposes (pink error bars). (a) Tumor radius, (b) tumor vessel surface area (SA), (c) proliferating tissue fraction, (d) hypoxic tissue fraction, (e) necrotic tissue fraction, (f) ratio of Type 1 to Type 2 macrophages (log₁₀ scale). Type 1 macrophages are not present in the HIGH case.



TABLE 3. Transformed and rescaled intensities and weighted coefficients for a representative sample

Metabolite	Tumor pro- liferation	Type 1 macrophage	Type 2 macrophage	Angio- genesis	Drug effect	Lactic acid production	Monocyte production	Transformed and rescaled intensities M_i
Acetyl- _L - carnitine ^A	0.0602	0	0	0.1854	0	0	0	1.13
N8-Acetyl- spermidine ^A	0.0571	0	0	0	0	0	0	2.59
Arginine ^A	0.0805	0.1392	0.1392	0	0	0	0	1.02
Creatinine ^A	0	0.1148	0.1148	0	0	0	0	0.56
Cystine ^B	0.0303	0	0	0	0	0	0	1.45
Fumarate ^B	0	0	0	0.1260	0.2559	0	0	2.16
Glutamic acid ^B	0	0	0	0	0.4090	0	0	0.48
Glutamine ^B	0.0766	0.1325	0.1325	0	0	0	0	0.20
Glutaric acid ^A	0.0381	0	0	0	0	0	0	0.15
Hydroxybutyric acid ^A	0.0547	0	0	0	0	0	0	1.66
Hydroxyphenyl- lactic acid ^A	0	0	0	0	0	0	0.1503	0.00
Inosine ^A	0.0738	0	0	0	0	0	0	1.88
Isoleucine ^B	0.0764	0	0	0	0	0	0	0.64
Lactic acid ^A	0	0	0	0.1028	0	0.4306	0	1.02
Lysine ^B	0.0411	0	0	0	0	0	0	0.51
Malonic acid ^A	0	0	0	0	0.3351	0	0	0.92
Methionine ^B	0.0753	0	0	0	0	0	0	1.18
Methionine Sul- foxide ^B	0	0	0	0	0	0.5694	0	0.65
N3,N4-Dimethyl- L-arginine ^B	0	0.1244	0.1244	0	0	0	0	0.63
Ornithine ^A	0	0	0	0	0	0	0.1323	1.11
Phenylalanine ^B	0	0.0510	0.0510	0	0	0	0	0.88
Proline ^A	0.0806	0	0	0.2485	0	0	0	1.31
Pyruvate ^A	0.1095	0	0	0.3373	0	0	0.3418	1.46
Salicylic acid ^A	0	0	0	0	0	0	0.2146	1.32
Serine ^B	0.0383	0.0663	0.0663	0	0	0	0	0.65
Succinate ^A	0	0.1103	0.1103	0	0	0	0	0.34
Threonine ^B	0	0.0764	0.0764	0	0	0	0	0.36
Tryptophan ^B	0	0.0592	0.0592	0	0	0	0	1.67
Urea ^B	0	0	0	0	0	0	0.1609	2.41
Uric acid ^A	0.0728	0.1259	0.1259	0	0	0	0	0.64
Valine ^B	0.0349	0	0	0	0	0	0	0.52

Transformed and rescaled intensity values for a representative sample and weighted coefficients, calculated for each metabolite associated with the model parameters using a combination of PLS-DA VIP scores and Spearman correlation coefficients. ^APromoting tumor progression; ^Bpromoting tumor control. The coefficients (either promoting (italic values) or abating (bold values) the associated parameters) were derived as described in **Methods** from the metabolomic data from the study in Ref. 53. The coefficients are rescaled to a positive scale, where a value of zero corresponds to the minimum, as described in Fig. 1.

the sum of all values relevant to the given parameter (Fig. 1, Step 2) (Table 3). Here, we chose a combination of PLS-DA VIP scores and Spearman correlation coefficients to illustrate the calculation of the weighted coefficients. A PLS-DA VIP score and Spearman correlation coefficient are calculated for every metabolite using the clinical patient response as the categorized outcome variable. After rescaling all correlation coefficients to a positive scale, these two values are multiplied together and represent the weight coefficient W. These are considered two different methods of assigning weight to metabolites, relevant to the patient clinical outcome. We choose both by multiplying

them to be inclusive, as using only a single method of assigning weight to metabolites could introduce bias into the parameter calculations.

For every model parameter in Table 3, $P_{\rm desired}$ is found by summing the multiplication of the metabolite intensity values for that patient by the respective weighted coefficients for pro-parameter metabolites (values in red) and subtracting the sum of the multiplication of the metabolite intensity values for that patient by the respective weighted coefficients for antiparameter metabolites (values in blue). (Fig. 1, Step 3). $P_{\rm max}$ and $P_{\rm min}$ are respectively calculated using the maximum pro-parameter and minimum anti-parame-



ter, and the minimum pro-parameter and maximum anti-parameter metabolite intensities in the dataset (Fig. 1, Step 4). Next, the non-dimensionalized y-co-ordinate P_y values for each model parameter are determined from $P_{\rm desired}$, $P_{\rm min}$ and $P_{\rm max}$ (Fig. 1, Step 5). Lastly, the model parameter values are found as the x-coordinate values corresponding to each P_y in Fig. 2. The resulting values for the sample case are in Table 4.

The tumor behavior simulated by the model with these parameter values is in Fig. 3 and compared at 400 h in Fig. 4, showing that for this sample set of metabolite intensity values, the tumor radius would fall between the BASELINE and HIGH tumor radii. A consistent pattern from LOW to HIGH was observed for tumor radius, tumor vessel surface area, and proliferating and necrotic tissue fractions with HIGH, SAMPLE, MEDIUM, and LOW cases. The LOW case had decreased hypoxic fraction along with low vascularization, reflecting the values to represent low metabolic dysregulation in Table 2, including a low proliferation rate.

Note that the LOW and HIGH cases are used to define a range of NSCLC metabolic dysregulation within the limits of the corresponding model parameter (Table 2). Individual SAMPLE parameters, however, are calibrated to actual metabolomic data, which can yield combinations of parameter values that elicit tumor behavior outside of the range of the behavior elicited by the LOW and HIGH cases. In other words, an ordered set of values in the model parameter space does not necessarily yield a correspondingly ordered set of tumor behavior, since this behavior can be highly nonlinear.

Simulation of Chemotherapy Response

The metabolomic data from the study in 53 were used to calculate tumor model parameters for each patient, including the drug effect $\bar{\lambda}_{\text{effect}}$, and perform simulations of chemotherapy to assess the consistency of the expected response with each clinical classifica-

tion. Clinical outcomes included complete response (CR), partial response (PR), stable disease (SD) and progressive disease (PD). The patient classifications of CR/PR vs. SD/PD as well as disease control (DC: CR/ PR/SD) vs. PD were evaluated. In Fig. 5a, there was a significant difference in the average log-transformed anti-parameter metabolite intensity between CR/PR vs. SD/PD as well as DC vs. PD patient groups, while the average log-transformed pro-parameter metabolite intensity trended higher in SD/PD and PD patients compared to CR/PR and DC, respectively. In Fig. 5b, the results of simulating bolus drug injection in the patient cohort are shown at 3.4 days post-treatment in terms of tumor radius area-under-curve (AUC) and fraction of initial tumor radius. In all cases, there was a significant difference between responders (CR/PR and DC) and non-responders (SD/PD and PD), indicating that the model-simulated responses were able to classify the patient groups consistent with the clinical response based on the hypothesized linking of metabolite intensities to the model parameters (Table 1).

DISCUSSION

This study develops a method to link clinically measureable metabolomic data to tissue-scale tumor behavior. The tumor model representation is modulated by key parameters influencing cell proliferation, tumor tissue vascularization, monocyte infiltration, tumor-associated macrophage polarization, lactic acid production, and drug effect. These parameters interact with each other nonlinearly to influence the simulated tumor progression. A dynamic range for these parameters is established using NSCLC as a representative cancer in order to enable representation of low to high metabolically active tumors. This approach enables the simulation of tumor progression based on particular metabolomic measurements. Metabolomic data obtained from a set of patients undergoing lung

TABLE 4.	Model	narameter	values	for a	representative sample.
IADEL 4.	MOGE	parameter	values	ioi a	representative sample.

Parameter	P_{max}	$P_{\rm desired}$	P_{min}	P_{y}	Parameter value
Proliferation rate	1.650	0.584	- 0.844	0.573	1.357
Type 1 macrophage polarization constant	1.675	0.439	- 0.343	0.388	4.980
Type 2 macrophage polarization constant	0.343	- 0.439	- 1.675	0.612	8.076
Angiogenesis rate ^a	2.437	1.406	0.000	0.577	66.7
Lactic acid production rate ^a	0.999	0.071	- 0.816	0.489	192.4
Monocyte production rate	0.470	- 0.542	- 1.804	0.555	0.028
Drug effect constant	2.011	0.443	- 0.831	0.448	426.3

 P_{max} , P_{desired} , P_{min} values along with the corresponding model parameter values calculated for a representative sample from a metabolomic dataset using the proposed method. Metabolomic data were obtained from the study in Ref. 53.

^aParameter value is shown as % of the corresponding value for the baseline tumor.



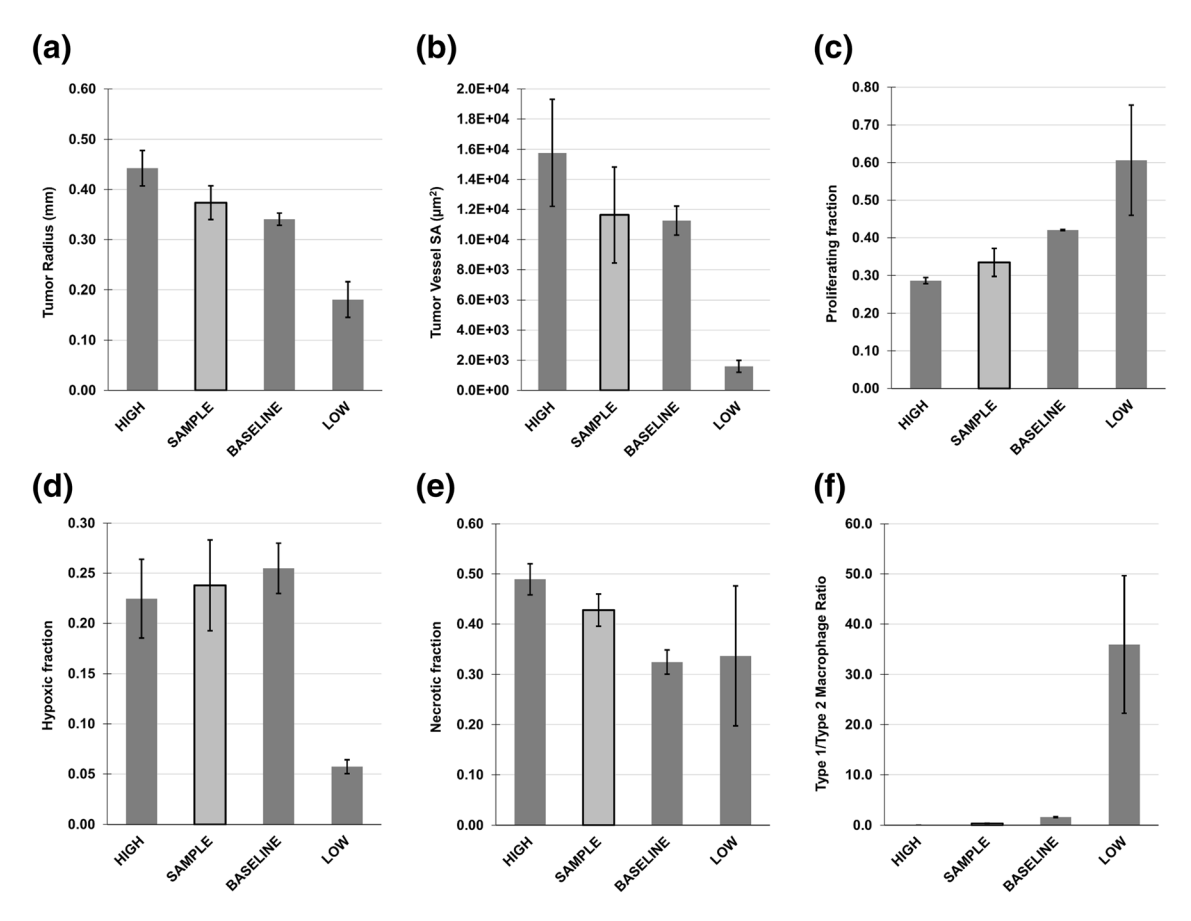


FIGURE 4. Tumor characteristics compared between different levels of metabolic dysregulation. Comparison is at 400 h, by which time a steady rate of growth was achieved. LOW: minimum theoretical dysregulation; BASELINE: dysregulation based on baseline tumor values; HIGH: maximum theoretical dysregulation; SAMPLE: a representative patient case for illustration purposes. (a) Tumor radius, (b) tumor vessel surface area (SA), (c) proliferating tissue fraction, (d) hypoxic tissue fraction, (e) necrotic tissue fraction, (f) ratio of Type 1 to Type 2 macrophages.

tumor core biopsies is used to show the feasibility of this approach.

Previous work has explored statistical approaches (e.g., machine learning) and network-oriented techniques (e.g., principal network analysis) to link the metabolome to tumor tissue-scale behavior; however, results based on these approaches may not necessarily represent any particular tumor. 55,59 Although some supervised learning methods (such as PLS-DA) trained with chemotherapy response data can be used to predict the outcome of chemotherapy for new patients, they are limited in that they are only trained by the set of predictor variables (here, the metabolomic data). The application of a mechanistically-based spatiotemporal model of tumor growth to simulate chemotherapy extends the predictive capacity of such statistical models and may provide insight into the mechanisms of treatment resistance. The system proposed here could recreate the behavior of particular tumors for in silico evaluation prior to treatment, incorporating patient tumor-specific metabolomic data. An approach combining data-driven multivariate statistical techniques (i.e., machine learning) with mechanistic spatiotemporal tissue modeling may be advantageous compared to using either one alone.

Previous studies have sought to find robust metabolic biomarkers related to cancer diagnosis, prognosis, and chemotherapeutic efficacy (e.g., Refs. 5, 44, 59, 69, 86). With a few exceptions, 18,62,63 the linking of metabolomic data to tissue-scale behavior has been lacking. Since cancer is a heterogeneous disease, one advantage of using a spatiotemporal mechanistic model is the ability to simulate in time different proportions of proliferating, hypoxic and necrotic tissue within the tumor tissue. 51 This can occur with varying vascular densities due to the surrounding host tissue, causing heterogeneous oxygen distribution. Differences in vasculature between tumors are expected to affect the delivery and distribution of chemotherapeutics administered intravenously.⁵¹ In previous work, chemotherapeutic efficacy has been determined in non-specific tumors. 16,17,51,52 Here, we use metabolic



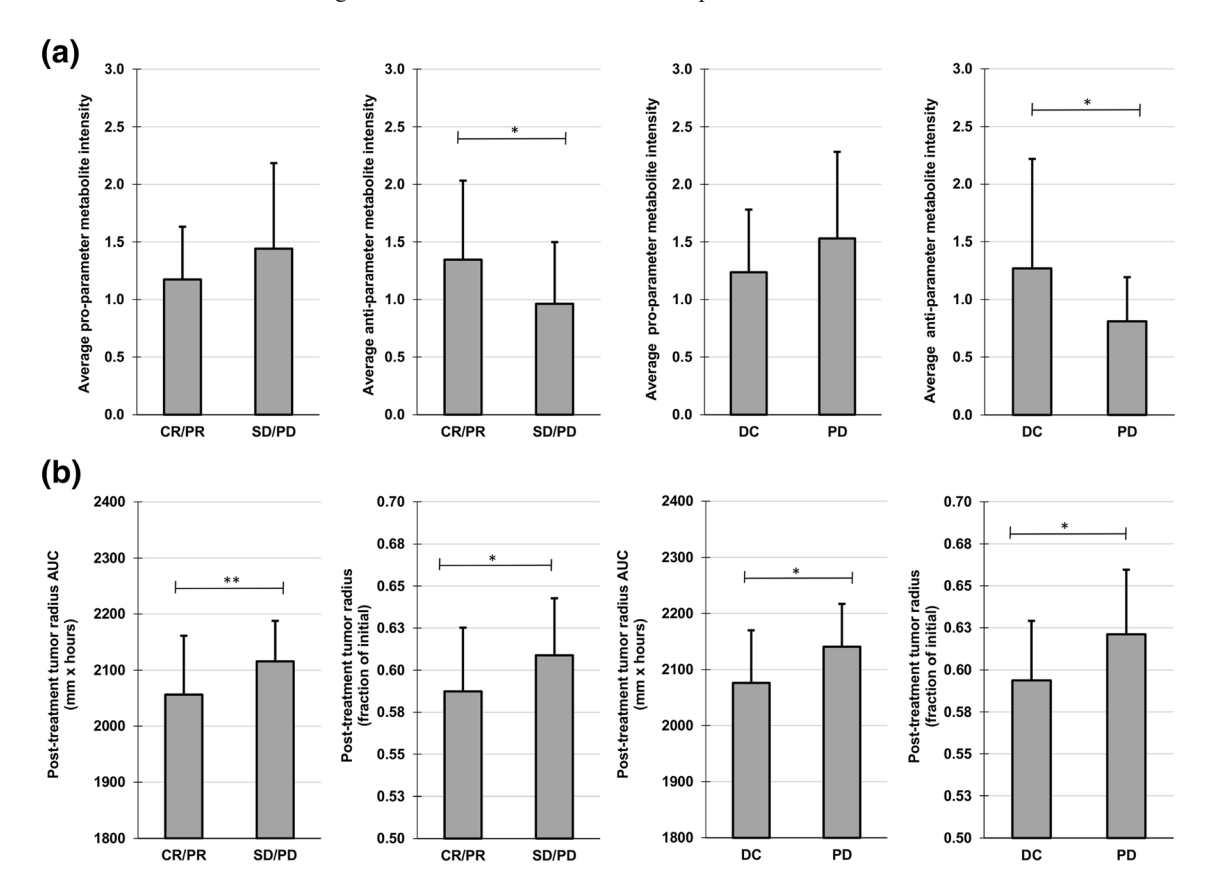


FIGURE 5. Patient classification based on chemotherapy response. (a) Average log transformed metabolite intensities for patients with clinical therapeutic response data, classified as CR/PR (complete response/partial response), SD/PD (stable disease/progressive disease), DC (disease control = CR/PR/SD) or progressive disease (PD). (b) Simulated post-treatment tumor radius AUC and post-treatment tumor radius (fraction of initial) after bolus injection of drug for responders (CR/PR and DC) and non-responders (SD/PD and PD). Simulated tumor metrics were measured at 3.4 days post-treatment (n = 3). * $p \le 0.05$; ** $p \le 0.01$.

characteristics to account for potential inter-patient differences in tumor vascularization, which through its effects influences the delivery and efficacy of chemotherapeutics.

Simulated patient tumor progression as a function of metabolomic data with the proposed methodology could differ from actual clinical results. The set of metabolites (Table 1) and the weighted coefficients assigned to them (Table 3) are critical in determining the model parameter values. The choice of metabolites depends on the specific cancer type and is determined from analysis of mass spectroscopy data for a set of patient data. As such, the set is expected to remain consistent for all patients with the same cancer type—in this study, NSCLC. However, the set may not be the same across different studies. For example, evaluating NSCLC patient plasma samples, eight metabolites were found to be associated with platinum chemotherapy response, 59 while seven metabolites were found in a study evaluating response to first-line chemotherapy of pemetrexed combined with either cisplatin or carboplatin.⁶⁹ Further, the weighted coefficients calculated via multivariate statistical techniques (i.e., machine learning) may be different depending on the

techniques chosen to calculate them, such as a neural network or pathway analysis combined with correlation analysis, which would potentially arrive at different weights for the same set of metabolites. Such differences highlight the need to validate any particular technique with actual outcomes observed in patients. It may also be relevant to explore how correlations between metabolites may affect the simulated results. Moreover, various combinations of model parameter values could give similar results. The parameter values reflect the overlapping of metabolites and tumor biological characteristics, and their combined effects on tumor progression. Although simulated tumor growth may be similar, it is expected that under therapy the results would be further affected by therapy-related parameters. Response to drugs other than cisplatin to reflect actual patient regimens should be evaluated. Additionally, the association of particular metabolites to model parameters (Table 1) depends on the state-of-the-art of the biological knowledge and the mass spectrometry (MS) analysis of the tissue samples. As metabolomic knowledge progresses, it is to be expected that the parameters may need to be calculated based on additional or different sets of



metabolites. Accordingly, the assumptions underlying their potential effects on the model parameters may need to be revisited. Care must also be taken to ensure that a consistent set of metabolites are captured during global metabolic profiling of patient biopsies across samples and analytical batches by using reliable state-of-the-art metabolite extraction techniques.

As the number of parameters required to discriminate between patients is unknown, it remains to be verified whether any particular set of parameters and their range of values can accurately simulate tumors from different patients. It may be necessary to augment the parameter set with further biologically-relevant information (e.g., immune cells other than macrophages) in order to achieve this goal. The range of values for the model parameters may also need to be expanded to accommodate the biological information, which could lead to redefinition of the scale describing metabolic dysregulation. A major constraint is that most of this type of information would be difficult to measure from individual tumor biopsies. Consequently, the model behavior depends mainly on the metabolomic information and how this information is weighted and combined to determine its effect on the model parameters. Using a small set of patient data, this study used parameter values linked to metabolite intensities modulated by weights and combinations based on clinical therapeutic responses to show consistency of the model simulated treatment responses with the clinical data. For future work, the weighting and combinations may need to be adjusted to fine-tune the system response to match what is observed with a larger test set of patient tumors, and then using this finer-calibrated system to predict the response for new patients. As a step towards this goal, this study establishes a framework to evaluate the complex interactions between metabolic parameters that drive tissue-scale tumor growth, providing a means to link the molecular- to the tissue-scale behavior.

SUPPLEMENTARY INFORMATION

The online version contains supplementary material available at https://doi.org/10.1007/s10439-022-02904-5.

ACKNOWLEDGMENTS

HBF acknowledges partial support by the National Institutes of Health/National Cancer Institute Grant R15CA203605. J.L. acknowledges partial support from NSF through Grants DMS-1714973 and the Simons Foundation (594598QN) for a NSF-Simons

Center for Multiscale Cell Fate Research. J.L. also thanks the National Institutes of Health for partial support through Grants 1U54CA217378-01A1 for a National Center in Cancer Systems Biology at UC Irvine and P30CA062203 for the Chao Family Comprehensive Cancer Center at UC Irvine.

CONFLICT OF INTEREST

The authors declare no known conflicts of interest.

REFERENCES

¹Abusalamah, H., J. M. Reel, and C. R. Lupfer. Pyruvate affects inflammatory responses of macrophages during influenza A virus infection. *Virus Res.* 286:198088, 2020.

²Adeva-Andany, M. M., L. Lopez-Maside, C. Donapetry-Garcia, C. Fernandez-Fernandez, and C. Sixto-Leal. Enzymes involved in branched-chain amino acid metabolism in humans. *Amino Acids*. 49:1005–1028, 2017.

³Ananieva, E. Targeting amino acid metabolism in cancer growth and anti-tumor immune response. *World J Biol Chem.* 6:281–289, 2015.

⁴Ananieva, E. A., and A. C. Wilkinson. Branched-chain amino acid metabolism in cancer. *Curr Opin Clin Nutr Metab Care*. 21:64–70, 2018.

⁵Armitage, E. G., and C. Barbas. Metabolomics in cancer biomarker discovery: current trends and future perspectives. *J Pharm Biomed Anal.* 87:1–11, 2014.

⁶Aspuria, P. P., S. Y. Lunt, L. Varemo, L. Vergnes, M. Gozo, J. A. Beach, B. Salumbides, K. Reue, W. R. Wiedemeyer, J. Nielsen, B. Y. Karlan, and S. Orsulic. Succinate dehydrogenase inhibition leads to epithelial-mesenchymal transition and reprogrammed carbon metabolism. *Cancer Metab.* 2:21, 2014.

⁷Bamji-Stocke, S., V. van Berkel, D. M. Miller, and H. B. Frieboes. A review of metabolism-associated biomarkers in lung cancer diagnosis and treatment. *Metabolomics*. 14:81, 2018.

⁸Bearer, E. L., J. S. Lowengrub, H. B. Frieboes, Y. L. Chuang, F. Jin, S. M. Wise, M. Ferrari, D. B. Agus, and V. Cristini. Multiparameter computational modeling of tumor invasion. *Cancer Res.* 69:4493–4501, 2009.

⁹Beloborodova, N., I. Bairamov, A. Olenin, V. Shubina, V. Teplova, and N. Fedotcheva. Effect of phenolic acids of microbial origin on production of reactive oxygen species in mitochondria and neutrophils. *J Biomed Sci.* 19:89, 2012.

¹⁰Chanmee, T., P. Ontong, K. Konno, and N. Itano. Tumorassociated macrophages as major players in the tumor microenvironment. *Cancers (Basel)*. 6:1670–1690, 2014.

¹¹Chen, J., R. A. Chaurio, C. Maueroder, A. Derer, M. Rauh, A. Kost, Y. Liu, X. Mo, A. Hueber, R. Bilyy, M. Herrmann, Y. Zhao, and L. E. Munoz. Inosine released from dying or dead cells stimulates cell proliferation via adenosine receptors. *Front Immunol*. 8:504, 2017.

¹²Cho, H. W., S. B. Kim, M. K. Jeong, Y. Park, N. G. Miller, T. R. Ziegler, and D. P. Jones. Discovery of metabolite features for the modelling and analysis of high-resolution NMR spectra. *Int J Data Min Bioinform*. 2:176–192, 2008.



¹³Combs, J. A., and G. M. DeNicola. The non-essential amino acid cysteine becomes essential for tumor proliferation and survival. *Cancers (Basel)*. 11:678, 2019.

¹⁴Cooke, J. P., and Y. T. Ghebremariam. Endothelial nicotinic acetylcholine receptors and angiogenesis. *Trends Cardiovasc Med.* 18:247–253, 2008.

¹⁵Cristini, V., H. B. Frieboes, R. Gatenby, S. Caserta, M. Ferrari, and J. Sinek. Morphologic instability and cancer invasion. *Clin Cancer Res.* 11:6772–6779, 2005.

¹⁶Curtis, L. T., C. G. England, M. Wu, J. Lowengrub, and H. B. Frieboes. An interdisciplinary computational/experimental approach to evaluate drug-loaded gold nanoparticle tumor cytotoxicity. *Nanomedicine (Lond)*. 11:197–216, 2016.

¹⁷Curtis, L. T., V. H. van Berkel, and H. B. Frieboes. Pharmacokinetic/pharmacodynamic modeling of combination-chemotherapy for lung cancer. *J Theor Biol*. 448:38–52, 2018.

¹⁸Daghir-Wojtkowiak, E., P. Wiczling, M. Waszczuk-Jankowska, R. Kaliszan, and M. J. Markuszewski. Multilevel pharmacokinetics-driven modeling of metabolomics data. *Metabolomics*. 13:31, 2017.

¹⁹de la Cruz-Lopez, K. G., L. J. Castro-Munoz, D. O. Reyes-Hernandez, A. Garcia-Carranca, and J. Manzo-Merino. Lactate in the regulation of tumor microenvironment and therapeutic approaches. *Front Oncol.* 9:1143, 2019.

²⁰Dutta, S., S. Ray, and K. Nagarajan. Glutamic acid as anticancer agent: an overview. *Saudi Pharm J.* 21:337–343, 2013.

²¹Eisenhauer, E. A., P. Therasse, J. Bogaerts, L. H. Schwartz, D. Sargent, R. Ford, J. Dancey, S. Arbuck, S. Gwyther, M. Mooney, L. Rubinstein, L. Shankar, L. Dodd, R. Kaplan, D. Lacombe, and J. Verweij. New response evaluation criteria in solid tumours: revised RECIST guideline (version 1.1). Eur J Cancer. 45:228–247, 2009.

²²Elia, I., D. Broekaert, S. Christen, R. Boon, E. Radaelli, M. F. Orth, C. Verfaillie, T. G. P. Grunewald, and S. M. Fendt. Proline metabolism supports metastasis formation and could be inhibited to selectively target metastasizing cancer cells. *Nat Commun.* 8:15267, 2017.

²³Fini, M. A., A. Elias, R. J. Johnson, and R. M. Wright. Contribution of uric acid to cancer risk, recurrence, and mortality. *Clin Transl Med.* 1:16, 2012.

²⁴Frieboes, H. B., X. Zheng, C. H. Sun, B. Tromberg, R. Gatenby, and V. Cristini. An integrated computational/experimental model of tumor invasion. *Cancer Res.* 66:1597–1604, 2006.

²⁵Habte-Tsion, H. M., M. Ren, B. Liu, X. Ge, J. Xie, and R. Chen. Threonine modulates immune response, antioxidant status and gene expressions of antioxidant enzymes and antioxidant-immune-cytokine-related signaling molecules in juvenile blunt snout bream (*Megalobrama ambly-cephala*). Fish Shellfish Immunol. 51:189–199, 2016.

²⁶Higuchi, S., Y. Osada, Y. Shioiri, N. Tanaka, S. Otomo, and H. Aihara. The modes of anti-inflammatory and analgesic actions of aspirin and salicylic acid. *Nihon Yakurigaku Zasshi*. 85:49–57, 1985.

²⁷Hilvo, M., I. de Santiago, P. Gopalacharyulu, W. D. Schmitt, J. Budczies, M. Kuhberg, M. Dietel, T. Aittokallio, F. Markowetz, C. Denkert, J. Sehouli, C. Frezza, S. Darb-Esfahani, and E. I. Braicu. Accumulated metabolites of hydroxybutyric acid serve as diagnostic and prognostic biomarkers of ovarian high-grade serous carcinomas. *Cancer Res.* 76:796–804, 2016.

²⁸Jung, S. Y., H. S. Song, S. Y. Park, S. H. Chung, and Y. J. Kim. Pyruvate promotes tumor angiogenesis through HIF-1-dependent PAI-1 expression. *Int J Oncol.* 38:571–576, 2011.

²⁹Kalluri, R., and R. A. Weinberg. The basics of epithelial-mesenchymal transition. *J Clin Invest*. 119:1420–1428, 2000

³⁰Kim, Y. S. Malonate metabolism: biochemistry, molecular biology, physiology, and industrial application. *J Biochem Mol Biol.* 35:443–451, 2002.

³¹Koppula, P., Y. Zhang, J. Shi, W. Li, and B. Gan. The glutamate/cystine antiporter SLC7A11/xCT enhances cancer cell dependency on glucose by exporting glutamate. *J Biol Chem.* 292:14240–14249, 2017.

³²Kratochvill, F., G. Neale, J. M. Haverkamp, L. A. Van de Velde, A. M. Smith, D. Kawauchi, J. McEvoy, M. F. Roussel, M. A. Dyer, J. E. Qualls, and P. J. Murray. TNF counterbalances the emergence of M2 tumor macrophages. *Cell Rep.* 12:1902–1914, 2015.

³³Lee, M., G. T. Chen, E. Puttock, K. Wang, R. A. Edwards, M. L. Waterman, and J. Lowengrub. Mathematical modeling links Wnt signaling to emergent patterns of metabolism in colon cancer. *Mol Syst Biol.* 13:912, 2017.

³⁴Lee, O., and P. J. O'Brien. Modifications of mitochondrial function by toxicants. *Comprehen Toxicol*. 1:411–445, 2010.

³⁵Leighl, N. B. Treatment paradigms for patients with metastatic non-small-cell lung cancer: first-, second-, and third-line. *Curr Oncol.* 19:S52-58, 2012.

³⁶Leonard, F., L. T. Curtis, A. R. Hamed, C. Zhang, E. Chau, D. Sieving, B. Godin, and H. B. Frieboes. Nonlinear response to cancer nanotherapy due to macrophage interactions revealed by mathematical modeling and evaluated in a murine model via CRISPR-modulated macrophage polarization. *Cancer Immunol Immunother*. 69:731–744, 2020.

³⁷Leonard, F., L. T. Curtis, M. J. Ware, T. Nosrat, X. Liu, K. Yokoi, H. B. Frieboes, and B. Godin. Macrophage polarization contributes to the anti-tumoral efficacy of mesoporous nanovectors loaded with albumin-bound paclitaxel. *Front Immunol.* 8:693, 2017.

³⁸Leonard, F., L. T. Curtis, P. Yesantharao, T. Tanei, J. F. Alexander, M. Wu, J. Lowengrub, X. Liu, M. Ferrari, K. Yokoi, H. B. Frieboes, and B. Godin. Enhanced performance of macrophage-encapsulated nanoparticle albumin-bound-paclitaxel in hypo-perfused cancer lesions. *Nanoscale*. 8:12544–12552, 2016.

³⁹Lim, J. M., G. Kim, and R. L. Levine. Methionine in proteins: it's not just for protein initiation anymore. *Neu*rochem Res. 44:247–257, 2019.

⁴⁰Ma, E. H., G. Bantug, T. Griss, S. Condotta, R. M. Johnson, B. Samborska, N. Mainolfi, V. Suri, H. Guak, M. L. Balmer, M. J. Verway, T. C. Raissi, H. Tsui, G. Boukhaled, S. H. da Costa, C. Frezza, C. M. Krawczyk, A. Friedman, M. Manfredi, M. J. Richer, C. Hess, and R. G. Jones. Serine is an essential metabolite for effector T cell expansion. *Cell Metab*. 25:345–357, 2017.

⁴¹Macklin, P., S. McDougall, A. R. Anderson, M. A. Chaplain, V. Cristini, and J. Lowengrub. Multiscale modelling and nonlinear simulation of vascular tumour growth. *J Math Biol.* 58:765–798, 2009.

⁴²Mahlbacher, G., L. T. Curtis, J. Lowengrub, and H. B. Frieboes. Mathematical modeling of tumor-associated macrophage interactions with the cancer microenvironment. *J. Immunotherapy Cancer*. 6:10, 2018.



⁴³Marx, V. Biology: the big challenges of big data. *Nature*. 498:255–260, 2013.

- ⁴⁴Mathe, E. A., A. D. Patterson, M. Haznadar, S. K. Manna, K. W. Krausz, E. D. Bowman, P. G. Shields, J. R. Idle, P. B. Smith, K. Anami, D. G. Kazandjian, E. Hatzakis, F. J. Gonzalez, and C. C. Harris. Noninvasive urinary metabolomic profiling identifies diagnostic and prognostic markers in lung cancer. *Cancer Res.* 74:3259–3270, 2014.
- ⁴⁵Mattaini, K. R., M. R. Sullivan, and M. G. Vander Heiden. The importance of serine metabolism in cancer. *J Cell Biol*. 214:249–257, 2016.
- ⁴⁶Mazzio, E. A., N. Boukli, N. Rivera, and K. F. Soliman. Pericellular pH homeostasis is a primary function of the Warburg effect: inversion of metabolic systems to control lactate steady state in tumor cells. *Cancer Sci.* 103:422–432, 2012.
- ⁴⁷McAuslan, B. R., W. Reilly, G. N. Hannan, K. Schindhelm, B. Milthorpe, and B. A. Saur. Induction of endothelial cell migration by proline analogs and its relevance to angiogenesis. *Exp Cell Res.* 176:248–257, 1988.
- ⁴⁸McDougall, S. R., A. R. Anderson, and M. A. Chaplain. Mathematical modelling of dynamic adaptive tumour-induced angiogenesis: clinical implications and therapeutic targeting strategies. *J Theor Biol.* 241:564–589, 2006.

⁴⁹Medina, M. A. Mathematical modeling of cancer metabolism. *Crit Rev Oncol Hematol*. 124:37–40, 2018.

- ⁵⁰Mendoza-Juez, B., A. Martinez-Gonzalez, G. F. Calvo, and V. M. Perez-Garcia. A mathematical model for the glucose-lactate metabolism of in vitro cancer cells. *Bull Math Biol.* 74:1125–1142, 2012.
- ⁵¹Miller, H. A., and H. B. Frieboes. Evaluation of drug-loaded gold nanoparticle cytotoxicity as a function of tumor vasculature-induced tissue heterogeneity. *Ann Biomed Eng.* 47:257–271, 2019.
- ⁵²Miller, H. A., and H. B. Frieboes. Pharmacokinetic/pharmacodynamics modeling of drug-loaded PLGA nanoparticles targeting heterogeneously vascularized tumor tissue. *Pharm Res.* 36:185, 2019.
- ⁵³Miller, H. A., X. Yin, S. A. Smith, X. Hu, X. Zhang, J. Yan, D. M. Miller, V. van Berkel, and H. B. Frieboes. Evaluation of disease staging and chemotherapeutic response in non-small cell lung cancer from patient tumor-derived metabolomic data. *Lung Cancer*. 156:20–30, 2021.
- ⁵⁴Moeslinger, T., R. Friedl, I. Volf, M. Brunner, H. Baran, E. Koller, and P. G. Spieckermann. Urea induces macrophage proliferation by inhibition of inducible nitric oxide synthesis. *Kidney Int.* 56:581–588, 1999.
- ⁵⁵Mucaki, E. J., J. Z. L. Zhao, D. J. Lizotte, and P. K. Rogan. Predicting responses to platin chemotherapy agents with biochemically-inspired machine learning. *Signal Transduct Target Ther.* 4:1, 2019.
- ⁵⁶Mudumba, S., A. Menezes, D. Fries, and J. Blankenship. Differentiation of PC12 cells induced by N8-acetylspermidine and by N8-acetylspermidine deacetylase inhibition. *Biochem Pharmacol.* 63:2011–2018, 2002.
- ⁵⁷Newman, A. C., and O. D. K. Maddocks. Serine and functional metabolites in cancer. *Trends Cell Biol.* 27:645– 657, 2017.
- ⁵⁸Patil, M. D., J. Bhaumik, S. Babykutty, U. C. Banerjee, and D. Fukumura. Arginine dependence of tumor cells: targeting a chink in cancer's armor. *Oncogene*. 35:4957–4972, 2016.
- ⁵⁹Peng, F., Y. Liu, C. He, Y. Kong, Q. Ouyang, X. Xie, T. Liu, Z. Liu, and J. Peng. Prediction of platinum-based

- chemotherapy efficacy in lung cancer based on LC-MS metabolomics approach. *J Pharm Biomed Anal.* 154:95–101 2018
- ⁶⁰Riesberg, L. A., T. L. McDonald, Y. Wang, X. M. Chen, S. W. Holzmer, S. M. Tracy, and K. M. Drescher. Creatinine downregulates TNF-alpha in macrophage and T cell lines. *Cytokine*. 110:29–38, 2018.
- ⁶¹Rodriguez, P. C., and A. C. Ochoa. T cell dysfunction in cancer: role of myeloid cells and tumor cells regulating amino acid availability and oxidative stress. *Semin Cancer Biol.* 16:66–72, 2006.
- ⁶²Roy, M., and S. D. Finley. Computational model predicts the effects of targeting cellular metabolism in pancreatic cancer. *Front Physiol.* 8:217, 2017.
- ⁶³Roy, M., and S. D. Finley. Metabolic reprogramming dynamics in tumor spheroids: Insights from a multicellular, multiscale model. *PLoS Comput Biol.* 15:e1007053, 2019.
- ⁶⁴San-Millan, I., and G. A. Brooks. Reexamining cancer metabolism: lactate production for carcinogenesis could be the purpose and explanation of the Warburg effect. *Carcinogenesis*. 38:119–133, 2017.
- ⁶⁵Sellers, K., M. P. Fox, M. Bousamra 2nd., S. P. Slone, R. M. Higashi, D. M. Miller, Y. Wang, J. Yan, M. O. Yuneva, R. Deshpande, A. N. Lane, and T. W. Fan. Pyruvate carboxylase is critical for non-small-cell lung cancer proliferation. *J Clin Invest*. 125:687–698, 2015.
- ⁶⁶Sikalidis, A. K. Amino acids and immune response: a role for cysteine, glutamine, phenylalanine, tryptophan and arginine in T-cell function and cancer? *Pathol Oncol Res.* 21:9–17, 2015.
- ⁶⁷Sriyudthsak, K., F. Shiraishi, and M. Y. Hirai. Mathematical modeling and dynamic simulation of metabolic reaction systems using metabolome time series data. *Front Mol Biosci.* 3:15, 2016.
- ⁶⁸Tantawy, A. A., and D. M. Naguib. Arginine, histidine and tryptophan: a new hope for cancer immunotherapy. *Phar-maNutrition*. 8:100148, 2019.
- ⁶⁹Tian, Y., Z. Wang, X. Liu, J. Duan, G. Feng, Y. Yin, J. Gu, Z. Chen, S. Gao, H. Bai, R. Wan, J. Jiang, J. Liu, C. Zhang, D. Wang, J. Han, X. Zhang, L. Cai, J. He, and J. Wang. Prediction of chemotherapeutic efficacy in non-small cell lung cancer by serum metabolomic profiling. *Clin Cancer Res.* 24:2100–2109, 2018.
- ⁷⁰van de Ven, A. L., M. Wu, J. Lowengrub, S. R. McDougall, M. A. Chaplain, V. Cristini, M. Ferrari, and H. B. Frieboes. Integrated intravital microscopy and mathematical modeling to optimize nanotherapeutics delivery to tumors. *AIP Adv.* 2:11208, 2012.
- ⁷¹van den Berg, R. A., H. C. Hoefsloot, J. A. Westerhuis, A. K. Smilde, and M. J. van der Werf. Centering, scaling, and transformations: improving the biological information content of metabolomics data. *BMC Genomics*. 7:142, 2006.
- ⁷²Wanders, D., K. Hobson, and X. Ji. Methionine restriction and cancer biology. *Nutrients*. 12:684, 2020.
- ⁷³Ware, M. J., L. T. Curtis, M. Wu, J. C. Ho, S. J. Corr, S. A. Curley, B. Godin, and H. B. Frieboes. Pancreatic adenocarcinoma response to chemotherapy enhanced with non-invasive radio frequency evaluated via an integrated experimental/computational approach. *Sci Rep.* 7:3437, 2017.
- ⁷⁴Watanabe, H., M. Okada, Y. Kaji, M. Satouchi, Y. Sato, Y. Yamabe, H. Onaya, M. Endo, M. Sone, and Y. Arai. New response evaluation criteria in solid tumours-revised



- RECIST guideline (version 1.1). Gan To Kagaku Ryoho. 36:2495–2501, 2009.
- ⁷⁵Wilmore, D. W., and J. K. Shabert. Role of glutamine in immunologic responses. *Nutrition*. 14:618–626, 1998.
- ⁷⁶Winkler, M. S., A. Nierhaus, G. Rosler, S. Lezius, O. Harlandt, E. Schwedhelm, R. H. Boger, and S. Kluge. Symmetrical (SDMA) and asymmetrical dimethylarginine (ADMA) in sepsis: high plasma levels as combined risk markers for sepsis survival. *Crit Care*. 22:216, 2018.
- ⁷⁷Wu, H., M. Ying, and X. Hu. Lactic acidosis switches cancer cells from aerobic glycolysis back to dominant oxidative phosphorylation. *Oncotarget*. 7:40621–40629, 2016.
- ⁷⁸Wu, J. Y., T. W. Huang, Y. T. Hsieh, Y. F. Wang, C. C. Yen, G. L. Lee, C. C. Yeh, Y. J. Peng, Y. Y. Kuo, H. T. Wen, H. C. Lin, C. W. Hsiao, K. K. Wu, H. J. Kung, Y. J. Hsu, and C. C. Kuo. Cancer-derived succinate promotes macrophage polarization and cancer metastasis via succinate receptor. *Mol Cell*. 77:213–227, 2020.
- ⁷⁹Wu, M., H. B. Frieboes, S. R. McDougall, M. A. Chaplain, V. Cristini, and J. Lowengrub. The effect of interstitial pressure on tumor growth: coupling with the blood and lymphatic vascular systems. *J Theor Biol.* 320:131–151, 2013.
- ⁸⁰Wu, Z., D. Wei, W. Gao, Y. Xu, Z. Hu, Z. Ma, C. Gao, X. Zhu, and Q. Li. TPO-induced metabolic reprogramming drives liver metastasis of colorectal cancer CD110+ tumor-initiating cells. *Cell Stem Cell*. 17:47–59, 2015.

- ⁸¹Yang, M., T. Soga, P. J. Pollard, and J. Adam. The emerging role of fumarate as an oncometabolite. *Front Oncol.* 2:85, 2012.
- ⁸²Yizhak, K., B. Chaneton, E. Gottlieb, and E. Ruppin. Modeling cancer metabolism on a genome scale. *Mol Syst Biol*. 11:817, 2015.
- ⁸³Yu, H., H. Xia, Q. Tang, H. Xu, G. Wei, Y. Chen, X. Dai, Q. Gong, and F. Bi. Acetylcholine acts through M3 muscarinic receptor to activate the EGFR signaling and promotes gastric cancer cell proliferation. *Sci Rep.* 7:40802, 2017
- ⁸⁴Yu, H. E., F. Wang, F. Yu, Z. L. Zeng, Y. Wang, Y. X. Lu, Y. Jin, D. S. Wang, M. Z. Qiu, H. Y. Pu, T. B. Kang, D. Xie, H. Q. Ju, R. H. Xu, and H. Y. Luo. Suppression of fumarate hydratase activity increases the efficacy of cisplatin-mediated chemotherapy in gastric cancer. *Cell Death Dis.* 10:413, 2019.
- ⁸⁵Yue, Y., W. Huang, J. Liang, J. Guo, J. Ji, Y. Yao, M. Zheng, Z. Cai, L. Lu, and J. Wang. IL4I1 is a novel regulator of m2 macrophage polarization that can inhibit T cell activation via L-tryptophan and arginine depletion and IL-10 production. *PLoS ONE*. 10:e0142979, 2015.
- ⁸⁶Zhang, A., H. Sun, G. Yan, P. Wang, Y. Han, and X. Wang. Metabolomics in diagnosis and biomarker discovery of colorectal cancer. *Cancer Lett.* 345:17–20, 2014.

Publisher's Note Springer Nature remains neutral with regard to jurisdictional claims in published maps and institutional affiliations.

